

# A pulsar outer gap model with trans- $\gamma$ structure

J. Takata,<sup>1?</sup> S. Shibata,<sup>2</sup> K. Hirokuni,<sup>3</sup>

<sup>1</sup> Graduate School of Science and Engineering, Yamagata University, Yamagata 990-8560, Japan

<sup>2</sup> Department of Physics, Yamagata University, Yamagata 990-8560, Japan

<sup>3</sup> Max-Planck-Institut fuer Kernphysik, Postfach 103980 D-69029 Heidelberg, Germany

## ABSTRACT

We investigate the electrodynamics of an outer gap in the meridional plane of the aligned-rotator. The charge depletion from the Goldreich-Julian charge density causes a large electric field along the magnetic field line. The electrons or the positrons are accelerated by the field-aligned electric field and radiate the  $\gamma$ -rays tangentially to the local magnetic field line. Some of such  $\gamma$ -rays collide with X-rays to materialize as the electron-positron pairs on different field lines from the field line on which they were emitted. As a result, the electric field structure is expected to change across the field lines. Including these trans- $\gamma$  effects, we solve the formation of the electric field self-consistently with the curvature radiation and the pair creation processes. The  $\gamma$ -ray emission and the pair creation are treated by use of Monte Carlo technique. We demonstrate that the distribution of the electric field along the field lines is affected by both the gap geometry and the external currents coming into the gap through the boundaries. In the electrodynamic model, it has been known that the solution disappears if the current density carried by the electron-positron pairs produced in the gap exceeds a critical value. We show that the critical current density is significantly increased when the trans- $\gamma$  structure is taken into account. We also find that the location of the inner boundary of the gap shifts toward the stellar surface from the conventional null surface as the current density increases. The reason for the shift is derived from the stability condition of the inner boundary. We also argue that the ideal-MHD condition holds outside of the gap only when the low energy particles coexist with the high energy particles migrating from the gap.

Key words: radiation mechanism; non-thermal method; analytical-pulsar;  
general- $\gamma$ -rays; theory

## 1 INTRODUCTION

The rotation-powered pulsars have been known as sources of pulsed radio emission. The Compton Gamma-Ray Observatory (CGRO) had shown that the young pulsars are also strong  $\gamma$ -ray sources, and had detected seven  $\gamma$ -ray pulsars (Thompson 1999). The CGRO revealed the fact that  $\gamma$ -ray luminosity accounts for about 10% of the spin down energy. Furthermore, the observations for the  $\gamma$ -ray spectra and light curves tell us a lot about acceleration of particles in the pulsar magnetosphere. The energy peak in the spectra above 1 GeV shows that the electrons or the positrons are accelerated above  $10^{12}$  eV. A pulsation in the observed light curves implies that the acceleration of the particles and the subsequent radiation take place within the light cylinder, the axial distance of which is given by  $r_{lc} = c/\omega$ , where  $\omega$  is the angular frequency, and  $c$  the speed of light. Although these observations provide constraints on proposed models, the origin of the  $\gamma$ -ray emission is not conclusive up to now.

The global model for the acceleration of the particles in the magnetosphere has been considered as follows. The pulsar is an electric dynamo of about  $10^{16}$  V. The resultant electromagnetic energy is carried into the magnetosphere by a longitudinal current. Then, if there is a large electric potential drop along the magnetic field, the current carriers (probably electrons and/or positrons) should be accelerated to high energies by the field-aligned electric field, and should release the electromagnetic energy by emitting  $\gamma$ -rays. If there were no electric potential drop along the magnetic field, the space charge in the magnetosphere should be the Goldreich-Julian charge density (Goldreich-Julian 1969, hereafter GJ),

$$\rho_{GJ} = -\frac{1}{2c} \mathbf{e}_z \cdot \nabla B \quad (r < r_{lc}); \quad (1)$$

where  $\mathbf{e}_z$  is the unit vector along the rotation axis, and  $B$  is the magnetic field. On the other hand, any charge depletions from the GJ value cause the field-aligned electric field  $E_{||}$ .

According to the above point of view, the acceleration of particles and the subsequent  $\gamma$ -ray emission have been argued with the polar cap model (Sturrock 1971; Ruderman & Sutherland 1975) and the outer gap model (Cheng, Ho & Ruderman 1986, hereafter CHR), the acceleration regions of which are, respectively, located near the stellar surface above the

magnetic poles and in the outer magnetosphere around the null charge surface ( $\phi_{GJ} = 0$ ) above the last open field lines. Because the magnetic geometry of the polar caps explains well the observed radio polarization, it is widely accepted that the radio emission occurs above the polar caps.

The outer gap model has been successful in explaining the observed light curves. By solving the Poisson equation for a vacuum gap, CHR concluded that the outer gap extends between the null surface and the light cylinder. With this vacuum gap geometry, the double peaks in the light curves can be interpreted as an effect of aberration and time delay of the emitted photons (Romani & Yadigaroglu 1995; Cheng, Ruderman & Zhang 2000). Although the spectrum has also been calculated with the models, in which  $\gamma$ -ray radiation has been calculated with an assumed field-aligned electric field, the models are not satisfactory in the sense of electrodynamics. Dyks & Rudak (2003) argued that the acceleration region extends to the stellar surface and the light cylinder to reproduce the observed outer-wing emission, and the  $\alpha$ -pulse emission in the Crab pulsar, questioning the traditional vacuum gap geometry.

A non-vacuum outer gap model was proposed by Hirota & Shibata (1999). They have focused on the electrodynamics, in which screening of the electric field by the electron-positron pairs is taken into account. In the traditional outer gap models such as Romani & Yadigaroglu (1995), distribution of the electric field was not determined in a self-consistent manner with the radiation and pair creation processes. Hirota & Shibata (1999) solved the field-aligned electric field self-consistently with the curvature radiation and the pair creation processes, although they worked in one-dimension along the last open field line (see also Hirota 2003 for recent version of the one-dimensional model). They argued that if there is an injection of the particles into the gap, the position of the gap changes outwardly or inwardly relative to the null surface (Hirota & Shibata 2001).

In these one-dimensional electrodynamical models, the current carried by pairs produced in the gap was restricted to be about 10% of the  $GJ$  value. So, the model does not account for the observed  $\gamma$ -ray fluxes of some pulsars, although reproducing the  $\gamma$ -spectra well (Hirota, Harding & Shibata 2003; Takata, Shibata & Hirota 2004). In the traditional outer gap model, on the other hand, the current densities are not calculated, but assumed to be the  $GJ$  values. The limitations on the current density and the  $\gamma$ -ray luminosity in the electrodynamical model may be due to one-dimensionality. It is obvious that the electrodynamics is affected by the trans-field effect such that the accelerated particles causes new pairs to

be created on different field lines from the residing field line as pointed by CHR. Furthermore, calculations for the light curves and the phase-resolved spectra require departure from the one-dimensional model. On these grounds, in this paper, we extend the one-dimensional electrodynamic model into a two-dimensional one.

The most important trans-field effect is caused by curved field lines. The  $\gamma$ -rays, which are emitted tangentially to the local field lines, may convert into the pairs on the different field lines from the field line on which they are emitted. In the present paper, to avoid additional complications by the three-dimension, we study a two-dimensional model. In the subsequent paper, we will extend the two-dimensional model to a three-dimensional one. Our aim is to see how the structure of the electric field, the current density, and the geometry of the gap are affected by the trans-field effect.

By neglecting the magnetic component generated by the current, we assume the dipole magnetic field, and we consider the electrodynamics in the meridional plane of an aligned-rotator. This treatment simplifies the problem mathematically. Although it has been pointed out that an aligned-rotator is not active, that is, there are no longitudinal currents circulating in the magnetosphere (Michel & Li 1999), the present framework of the aligned models will apply to nearly aligned-rotators with the longitudinal currents.

We find a solution in which the particles produced in the gap carry about 30% of the GJ current, which is significantly larger than the value ( $\sim 10\%$ ) obtained in the one-dimensional model. We also show that the inner boundary of the gap shifts toward the stellar surface as the current increases.

In §2, we present the basic equations for the electrodynamics in the gap, and describe the treatment for the pair creation process. In §3, we show the results, and then discuss firstly the electric structure of vacuum and secondly non-vacuum cases. We also discuss the position of the inner boundary of the gap. In the final section, we compare the results with the previous works. We also discuss the dynamics for outside of the gap.

In the following sections, we make statements not only about the aligned-rotators but also about inclined-rotators if applicable. For the sign of charge, we assume "parallel rotator", for which the polar-caps are negatively charged.

## 2 TWO-DIMENSIONAL OUTER GAP MODEL

The present scheme consists of three main parts as follows;

(1) Poisson equation (xx2.1) is solved numerically with proper boundary conditions to give the electric field,

(2) the continuity equation for the particles (xx2.2) with pair creation term is solved on every field line to give the space charge density,

(3) -ray field and pair creation rate are obtained by using Monte Carlo technique (xx2.3).

These processes are iterated until all quantities are self-consistent (xx2.4).

## 2.1 Poisson equation

If stationary condition ( $\partial_t + \partial_\phi = 0$ , where  $t$  and  $\phi$  are the time and the azimuth, respectively) is satisfied, that is, if there is no time variation of any quantities as seen in co-rotating system, then an electric field,

$$\mathbf{E} = -(\mathbf{e}_z \times \mathbf{r}) \frac{B}{c} - \nabla \phi_{nc} \quad (2)$$

is exerted at position  $\mathbf{r}$  (Mestel 1999). The electric field can be expressed as the sum of the corotational part,  $-(\mathbf{e}_z \times \mathbf{r}) \frac{B}{c}$ , and the non-corotational part,  $-\nabla \phi_{nc}$ .

Goldreich & Julian (1969) proposed that the pulsar magnetosphere is filled by plasmas, and that the corotational condition

$$\mathbf{E} \cdot \mathbf{e}_j = -\mathbf{e}_j \cdot \nabla \phi_{nc} = 0 \quad (3)$$

is satisfied, where  $\mathbf{e}_j = B/B_j$  is the unit vector along the field line. If the star crust is a rigid rotating perfect conductor, and if the condition (3) holds all the way along the field lines connecting the star and the region considered, then the uniform value of  $\phi_{nc}$  over the stellar surface propagates into the magnetosphere. We set an arbitrary constant for  $\phi_{nc}$  on the surface to be zero in the following. The electric field (2) becomes  $\mathbf{E} = -(\mathbf{e}_z \times \mathbf{r}) \frac{B}{c}$ , which leads directly to the corotational charge density (1).

In a charge depletion region, where the condition (3) does not hold,  $\mathbf{E} \cdot \mathbf{e}_j$ -acceleration is indicated in the equation (2),  $\mathbf{E} \cdot \mathbf{e}_j = -\mathbf{e}_j \cdot \nabla \phi_{nc} \neq 0$ . By substituting equation (2) in  $\nabla \cdot \mathbf{E} = 4\pi\rho$ , we obtain the Poisson equation of the non-corotational potential  $\phi_{nc}$ ,

$$\nabla^2 \phi_{nc} = -4\pi(\rho - \rho_{nc}); \quad (4)$$

where  $\rho$  is the space charge density, and  $\nabla^2$  is the Laplacian.

If the variation in the azimuthal direction is negligible, we may reduce (4) to

$$\nabla_{r,\phi}^2 \phi_{nc} = -4\pi(\rho - \rho_{nc}); \quad (5)$$

where  $\nabla_{\text{r}}$  represents  $(r; \theta)$ -parts of the Laplacian;  $r$  and  $\theta$  are the radius and the colatitude, respectively, in the spherical polar coordinates. This approximation is justified only if the gap dimension in the meridional plane is much smaller than that in the azimuthal direction. We must lose some effects with this simplification, but we retain the trans-field effect, on which we put most interest.

We adopt an orthogonal curvilinear coordinate system based on the dipole field lines. The coordinates  $(\xi; \eta)$  are defined by

$$\frac{r \sin^2 \theta}{\xi_{\text{lc}}} = \text{constant along a dipole field line} \quad ; \quad (6)$$

and

$$\frac{r \cos^{1/2} \theta}{\eta_{\text{lc}}} = \text{constant along a curved line} \quad (7)$$

perpendicular to the field lines ;

respectively, where  $r$  is the distance from the centre of the star, and  $\theta$  is the colatitude angle with respect to the rotational axis. The line  $\xi = 1$  draws the last open field line, which is tangent to the light cylinder, and  $\eta = 1$  corresponds to the magnetic axis or  $r = 1$ . The Laplacian becomes

$$\nabla_{\text{r}}^2 = \frac{3 \cos^2 \theta + 1}{\sin^6 \theta} \frac{\partial^2}{\partial \xi^2} + \frac{4}{\sin^6 \theta} \frac{\partial}{\partial \xi} + \frac{3 \cos^2 \theta + 1}{4 \cos^3 \theta} \frac{\partial^2}{\partial \eta^2} + \frac{3(3 \cos^2 \theta + 1)}{4 \cos^3 \theta} \frac{\partial}{\partial \eta} ; \quad (8)$$

The non-rotational electric field  $E_{\text{nco}}$  is obtained by

$$E_{\text{rj}} = \frac{\partial \phi_{\text{nco}}}{\partial s_{\text{rj}}} = \frac{p}{2 \xi_{\text{lc}} \cos^{3/2} \theta} \frac{\partial \phi_{\text{nco}}}{\partial \xi} ; \quad (9)$$

$$E_{\text{?}} = \frac{\partial \phi_{\text{nco}}}{\partial s_{\text{?}}} = \frac{p}{\xi_{\text{lc}} \sin^3 \theta} \frac{\partial \phi_{\text{nco}}}{\partial \eta} ; \quad (10)$$

where  $ds_{\text{rj}} = 2 \cos^{3/2} \theta = \frac{p}{3 \cos^2 \theta + 1} d\xi$  and  $ds_{\text{?}} = \sin^3 \theta = \frac{p}{3 \cos^2 \theta + 1} d\eta$  are the line elements along the field lines and the perpendicular curved lines, respectively. Since dipole field is curl-free, we use  $\nabla_{\text{GJ}} B_z = 2 \mu_0 c$  as the GJ charge density.

## 2.2 Continuity equations for particles

Let us denote velocity  $\mathbf{v}$  as

$$\mathbf{v} = v_{\text{rj}} \mathbf{e}_{\text{rj}} + v_{\text{d}} ; \quad (11)$$

where  $v_{\text{d}}$  is the drift velocity owing to the electric field in the gap. The drift velocity is separated into the corotational and the non-corotational parts,

$$v_d = v_\infty + c \frac{E_{n\infty}}{B^2} B; \quad (12)$$

where  $v_\infty = e_z \cdot r$ . In the later section (x4), we shall see that the magnitude of the non-corotational drift is negligibly small in comparison with the corotational drift. By using  $r \cdot (nv) = B \cdot r_{\text{eff}}(vB) + \partial n / \partial t$  and imposing the stationary condition ( $\partial_t + \partial_r = 0$ ), the continuity equations become

$$B \cdot r \frac{v_{\text{eff}} N}{B} = S(r); \quad (13)$$

where  $S(r)$  is the source term due to the pair creation,  $N_+$  and  $N_-$  denote the number density of outwardly and inwardly moving particles, respectively. We suppose that the accelerated particles have almost the speed of light,  $v^2 = v_{\text{eff}}^2 + v_\infty^2 \approx c^2$ , such that the parallel component is assumed to be  $v_{\text{eff}} = \frac{c}{\sqrt{1 - \beta^2}}$ . With this parallel motion, the continuity equations (13) yield the particle's number density, provided that the source term  $S(r)$  is given.

If one assumes that the particle's motion immediately saturates in balance between the electric and the radiation reaction forces, the Lorentz factor of the particles within the gap is simply given by

$$\gamma_{\text{sat}}(r) = \frac{3R_c^2}{2e} E_{\text{eff}} + 1; \quad (14)$$

where  $R_c$  is the curvature radius of the magnetic field line. This saturation simplifies the problem significantly. However, the particles in the gap will have the saturated Lorentz factor  $\gamma_{\text{sat}}$  only when typical accelerating time  $t_{\text{ac}}$ , radiation damping time  $t_d$  and crossing time  $t_{\text{cr}} = W_{\text{eff}}/c$ , where  $W_{\text{eff}}$  is the gap width along the magnetic field lines, satisfy the condition,

$$t_{\text{cr}} \gg t_{\text{ac}} \text{ and } t_{\text{cr}} \gg t_d; \quad (15)$$

Hirohata, Harding & Shibata (2003), who solved unsaturated motion of the particles, showed that the condition  $t_{\text{cr}} \gg t_{\text{ac}}$  is not satisfied effectively for some pulsars. Although the unsaturated motion affects the  $\gamma$ -ray spectrum below 1 GeV (Hirohata et al. 2003; Takata et al. 2004), effect on the electric field is less important. As far as the electrodynamics are concerned, the assumption of the saturation will provide a good approximation.

The source term can be expressed as

$$S(r) = \int_0^{\infty} d\epsilon [\gamma_+ G_+ + \gamma_- G_-]; \quad (16)$$

where  $\epsilon$  is the photon energy normalized by  $m_e c^2$ ,  $G_+$  and  $G_-$  denote the distribution function of outwardly and inwardly propagating  $\gamma$ -rays. The pair creation rate  $\dot{\gamma}$  per unit time per  $\gamma$ -ray photon with the energy of  $\epsilon$  is given by

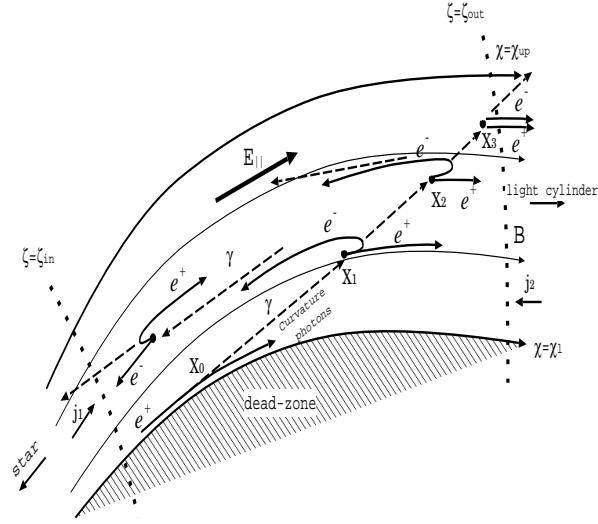


Figure 1. The pair creation cascade model in the meridional plane. The  $\gamma$ -rays are radiated by the curvature process, and are beamed in the direction of local magnetic field. The radiated  $\gamma$ -rays may convert into the pairs by the pair creation process. The  $\chi_{down}$ ,  $\chi_{up}$ ,  $\zeta_{in}$ , and  $\zeta_{out}$  present the lower, upper, inner, and outer boundaries of the gap, respectively.

$$p = (1 - \cos^2 \theta_c) c \int_{\chi_{th}}^{\chi_{up}} d\chi \frac{dN_X}{d\chi} p; \quad (17)$$

where  $d\chi = dN_X/d\chi$  is the X-ray number density between energies  $m_e c^2 \chi$  and  $m_e c^2 (\chi + d\chi)$ ,  $\cos^{-1} \theta_c$  is the collision angle between a X-ray and a  $\gamma$ -ray,  $m_e c^2 \chi_{th} = 2m_e c^2 = (1 - \cos^2 \theta_c)$  is the threshold X-ray energy for the pair creation, and  $p$  is the pair creation cross-section, which is given by

$$p(\chi; \chi_X) = \frac{3}{16} \pi (1 - \beta^2) (3 - \beta^4) \ln \frac{1 + \beta}{1 - \beta} - 2\beta (2 - \beta^2); \quad (18)$$

where

$$\beta(\chi; \chi_X) = \frac{s}{1 - \frac{2}{1 - \cos^2 \theta_c} \frac{1}{\chi}};$$

and  $\pi$  is the Thomson cross section.

In this paper, we take the blackbody radiation from the star as the X-ray field. At the distance  $r$ , the photon number density is given by the Planck law,

$$\frac{dN_X}{d\chi} = \frac{1}{4} \frac{2 m_e c^2 \chi^3}{h} \frac{A_s}{4 r^2} \frac{1}{\exp(m_e c^2 \chi / k T_s) + 1}; \quad (19)$$

where  $A_s$  is the emitting area, and  $k T_s$  refers to the surface temperature. For the values of  $A_s$  and  $T_s$ , observed ones may be used.

### 2.3 Pair creation model

We calculate  $S(r)$  by simulating the pair creation process with Monte Carlo method.

Fig.1 shows the pair creation cascade model schematically. Accelerated particles emit



rays tangentially to the local field lines by the curvature process. The rays deviate from the field line on which they are emitted. A small fraction of the emitted rays may collide with the X-ray photons to materialize as electron-positron pairs. For example,  $G_0$  photons emitted at position  $X_0$  in Fig.1 materialize as  $N_1, N_2$  pairs at positions  $X_1, X_2$ , respectively. The newborn electron-positron pairs such as the pairs depicted at the position  $X_1$  and  $X_2$ , will be separated immediately by the field-aligned electric field after their birth. The separated pairs also radiate the rays which become new seeds of a sequence of pair creations. The separated pairs carry a current, and provide a space charge to screen out the electric field.

On the other hand, as would be expected near the upper boundary of the gap, if the potential drop along the field lines is too small to separate a pair, then the pair would go out the gap together, such as pair depicted at position  $X_3$ . This kind of pairs does not affect the electrodynamics in the gap, in spite of the fact that they are produced in the gap. The pairs produced outside of the gap do not affect the dynamics either, because they do not directly come into the gap.

To obtain the source term  $S(r)$  at each position, we calculate the annihilated photon number  $N$  at the position  $r$ . In terms of mean free path of a ray with energy  $\epsilon$ ,  $l_p(r; \epsilon) = c/\nu_p(r; \epsilon)$ , the number of annihilated rays (produced pairs) between the distances  $s$  and  $s + ds$  from the emission point ( $s = 0$ ) is

$$N = \frac{G_0}{l_p} \exp \left[ -\int_0^s \frac{1}{l_p} ds' \right] ds \quad (20)$$

For the typical pulsar parameters, the mean free path  $l_p$  is found to be much longer than the light radius,  $l_p \gg r_{lc}$ , so that we can approximate equation (20) as  $N \approx (G_0/l_p)ds$ . We assume that  $l_p$  does not depend on the position, taking the value at  $r = 0.5r_{lc}$  with the collision angle  $\theta = 2$  ( $\theta_c = 0$ ). This assumption is probably a rough treatment because the X-ray number density (19) decreases with the distance from the centre of the star. In the present model, the pair creation position is given by uniform random number for the given element of the ray flux. It is notable that the rays are beamed in the direction of local particle's motion  $\mathbf{v} = v_{\parallel}\mathbf{e}_{\parallel} + v_{\perp}\mathbf{e}_{\perp}$ , so that an angle between the direction of the propagation and the meridional plane is  $\theta = \cos^{-1} \left[ \frac{v_{\parallel}}{v} \right] = \cos^{-1} \left[ \frac{v_{\parallel}}{v_{\perp}} \left( \frac{r}{r_{lc}} \right)^2 \right]$ . Hence, the displacement in the meridional plane is reduced to be  $s \cos \theta$ , where  $s$  is the three-dimensional path length of the rays.

Using the above pair creation model, the source term  $S(r)$  is obtained by the following

procedure (see also Fig.1). 1) We calculate the number  $G_0$  of the emitted photons per unit time per unit volume at the position  $X_0$ . 2) We calculate the number of photons converted into pairs in a distance  $s_0$  ( $\leq s_{lc}$ ) by  $G = G_0 [1 - \exp(-\int_0^{s_0} \Gamma ds)]$ . 3) We divide the  $G$  photons into  $n$  flux elements, and pick up  $n$  points on the three-dimensional path length ( $s_i < s_0; i = 1; \dots; n$ ) randomly. The pair creation points in the meridional plane are deduced from  $X_i - X_0 = s_i \cos \theta$ . 4) We calculate the produced pairs per unit time per unit volume as the source term  $S(X_i)$ . If potential drop between a pair creation point and boundaries is small ( $e \phi_{\infty} < 10^3 m_e c^2$  in this paper), we do not count the pair as the source. The emitting points of the  $\gamma$ -rays are scanned along the field line (from the inner boundary to the outer boundary) and across the magnetic field lines (from the lower boundary to the upper boundary). This direction of scanning across the field lines has an advantage because the  $\gamma$ -rays propagate always in convex side of the field lines. The particle's number density along the magnetic field line follows the equation (13). For the simplest treatment, all the curvature photons are assumed to be emitted at the critical energy,

$$E_c = \frac{3}{4} \frac{hc}{R_c} = 0.1 \frac{1}{100 s^{-1}} \frac{1}{10^7} \left( \frac{R_c}{s_{lc}} \right)^{-1} \text{ GeV}; \quad (21)$$

with the rate,

$$P = \frac{8}{9} \frac{e^2}{h R_c} = 3.2 \times 10^6 \frac{1}{10^7} \left( \frac{R_c}{s_{lc}} \right)^{-1} s^{-1}; \quad (22)$$

We introduce the conventional dimensionless variables;

$$r = \frac{r_p}{c}; \quad \Gamma_p = \frac{4}{m_e} \frac{e^2}{2 c \phi} \frac{B_{lc}}{\phi}; \quad (23)$$

$$\tilde{\phi}_{\infty} = \frac{e}{m_e c^2} \phi_{\infty}; \quad \tilde{E} = \tilde{r} \tilde{\phi}_{\infty}; \quad (24)$$

$$j = \frac{ev_{jj} N}{B=2}; \quad \tilde{B} = B/B_{lc}; \quad (25)$$

and

$$\tilde{v} = \frac{v}{c}; \quad (26)$$

where  $B_{lc}$  is the strength of the magnetic field at the point on which the last open field line is tangent to the light cylinder. By using dimensionless charge density,

$$\tilde{\rho} = \frac{\rho}{B_{lc}=2/c} = \frac{\tilde{B}}{j_{jj}} (j_+ - j_-); \quad \tilde{\gamma}_{GJ} = \tilde{B}_z; \quad (27)$$

the Poisson equation (4) and the continuity equation (13) are rewritten as

$$4 \tilde{\rho}_{\infty} = \frac{\tilde{B}}{j_{jj}} (j_+ - j_-) + \tilde{B}_z; \quad (28)$$

and

$$\tilde{B}(\tilde{r}_j) = S(r); \quad (29)$$

respectively.

## 2.4 Boundary conditions and method of calculation

We assume that the lower and the upper boundaries are laid on the magnetic surfaces labeled by  $\psi_1$  and  $\psi_{up}$ , respectively. The inner and the outer boundaries are defined by the surface on which  $E_{\parallel}$  vanishes,

$$E_{\parallel}(\psi_{in}) = E_{\parallel}(\psi_{out}) = 0; \quad (30)$$

where  $\psi_{in}$  and  $\psi_{out}$ , which are in general function of  $r$ , denote the location of the inner and the outer boundaries, respectively (Fig.1).

The conventional polar cap and outer gap models have their current densities flowing in opposite directions to each other. For this difference, it is impossible that these two acceleration regions are located on the same magnetic field lines. Therefore, we anticipate that the inner, the upper and the lower boundaries are directly linked with the star without any potential drop. We then impose

$$\tilde{n}_{\infty}(\psi_{in}) = \tilde{n}_{\infty}(\psi_{up}) = \tilde{n}_{\infty}(\psi_1) = 0; \quad (31)$$

The conditions (30) and (31) are not satisfied on arbitrary given boundaries, because both the Dirichlet-type and the Neumann-type conditions are imposed on the inner boundary  $\psi_{in}(\cdot)$ . We, therefore, solve the location of the inner boundary. By moving the inner boundary step by step iteratively, we seek for the boundary that satisfies the required conditions.

We have to consider the stability of the gap. The stability condition for the inner boundary is  $\partial E_{\parallel} / \partial s_{\parallel} > 0$  such that external electrons may not freely come into the gap through the inner boundary. This is similar to the force-free surface in the quiet aligned model by Michel (1979). In the same way, for the outer boundary it is  $\partial E_{\parallel} / \partial s_{\parallel} \leq 0$ . Furthermore, we postulate that the gap is unstable if the field-aligned electric field changes its direction. In other words, the sign of the field-aligned electric field is positive definite, as it guarantees that the positrons and the electrons propagate outwardly and inwardly, respectively. For the non-vacuum case, if super-GJ ( $j_{\parallel} > j_{GJ}$ ) region is dominant in the gap, then the electric field may change its direction.

The continuity equation (29) satisfies conservation law of the longitudinal current density, that is,

$$j_{\text{tot}} = j_g + j = \text{const along field line}; \quad (32)$$

where  $j_{\text{tot}}$  is the total current density in units of the  $G/J$  value. The total current is made up of the three components,

- (1)  $j_g$ , the current carried by the electrons and the positrons produced in the gap,
- (2)  $j_1$ , the current carried by the positrons (e.g. originating in sparking on the stellar surface) coming into the gap through the inner boundary,
- (3)  $j_2$ , the current carried by the electrons (e.g. originating in pulsar wind region) coming into the gap through the outer boundary.

We cannot deduce the value of  $j_{\text{tot}}$  from any gap model, because the current circulates in the magnetosphere globally. The outer gap, the polar cap and the pulsar wind may interact each other through the current, so that the current should be determined by some global conditions. In our local model, therefore, we regard the values of  $(j_g; j_1; j_2)$  as a set of free parameters. The boundary conditions on the current at the inner and the outer boundaries are given by

$$j_+ (r_{\text{in}}) = j_1 (r_{\text{in}}); \quad (33)$$

and

$$j_- (r_{\text{out}}) = j_2 (r_{\text{out}}); \quad (34)$$

respectively. In terms of  $(j_g; j_1; j_2)$ , the conservation law (32) yields

$$j_1 + j_2 + j_g = j_{\text{tot}}; \quad (35)$$

As has been mentioned, any local model should have some degrees of freedom because the model includes global quantities such as the electric current. The free parameters cannot be eliminated unless one solves the interaction with other parts of the magnetosphere (e.g. with pulsar wind). Furthermore, we have the free boundary problem with both the Dirichlet-type and the Neumann-type conditions. Hence, choice of a set of free model parameters is somewhat arbitrary. For convenience for the iteration, we choose the model parameters as follows. The external current sources  $(j_1; j_2)$  are obviously suitable to be free (e.g., in the traditional gap models, one assumes  $j_1 = j_2 = 0$ ). The lower boundary would be chosen as a model parameter, but it is traditionally set to be the last open field line, that is,  $r_1 = 1$ . We

give also the locations of the upper boundary  $r_{up}$  and the outer boundary  $r_{out}(\theta)$ , thereby we obtain a specific outer gap, namely we solve  $j_g(\theta)$  and the location of the inner boundary  $r_{in}(\theta)$ . Giving different  $r_{out}(\theta)$  and  $r_{up}$ , we obtain a series of models for which  $j_g(\theta)$  and  $r_{in}(\theta)$  are obtained.

One specific solution is determined by iteratively as follows. 1) By assuming the eld-aligned electric eld  $E_{jj}$  and the position of inner boundary  $r_{in}(\theta)$ , we start our calculation. 2) We calculate the particle's Lorentz factor (14) from  $E_{jj}$ . 3) We solve the curvature radiation and the pair creation processes by the method described in xx2.3, and then obtain the particle's number density in the gap. 4) Having the space charge density, we solve the Poisson equation to obtain new eld-aligned electric eld and the inner boundary that satisfies the required conditions. 5) We repeat 2)-4) until all the physical quantities are self-consistent.

The values of all the physical quantities go quickly toward convergence through the iteration. For example, if the eld-aligned electric eld is over estimated, then the resultant particle's number (or charge) density calculated with the radiation and the pair creation processes becomes larger than the solution. With this over estimated number density, however, the Poisson equation gives a smaller electric eld in the next step.

### 3 RESULTS

#### 3.1 Model parameters

As described in the last section, we take  $(j_1; j_2)$ ,  $(r_1; r_{up})$  and  $r_{out}$  as the model parameters. We  $x_1 = 1$  (i.e. the lower boundary is the last open eld line), and  $r_{out} = 1.6$  such that the trans-eld path length of  $\gamma$ -rays in the gap may becomes significant. To examine the effect of variation in the external current, we consider the following four cases;

Case 1:  $(j_1; j_2) = (0.0; 0.0)$  for  $r_{up} > r_0$ , but  $(j_1; j_2) = (10^{-5}; 10^{-5})$  for  $r_0 > r_1$ , where  $r_0 = r_1 + 0.02(r_{up} - r_1)$ ,

Case 2:  $(j_1; j_2) = (0.1; 0.1)$  for  $r_{up} > r_1$ ,

Case 3:  $(j_1; j_2) = (0.2; 0.0)$  for  $r_{up} > r_1$ ,

Case 4:  $(j_1; j_2) = (0.0; 0.2)$  for  $r_{up} > r_1$ .

In Case 2, the positronic and the electronic currents of 10% of the typical  $GJ$  value are injected into the gap from the inner and the outer boundaries, respectively. In Case 3 (or Case 4), on the other hand, the only positronic (or electronic) current comes into the gap

through either side of the gap. In Case 1, we consider the case of no external current, that is, the whole current is carried by the pairs produced in the gap. Because we need seed  $\gamma$ -rays to start the pair creation cascade in Case 1, we assume a very little currents ( $j_1 = j_2 = 10^{-5}$ ) in a thin layer (2% of the trans-field thickness) just above the last open field line.

In general,  $j_g$  increases with  $r_{up}$  (i.e. with the trans-field thickness). But, if  $j_g$  becomes larger than a critical value, we cannot get the stable solutions because the field-aligned electric field changes its sign in the gap. In this paper, we regard the maximized  $r_{up}$  as a natural boundary, and thereby we obtain  $r_{up} = 1.22$  (Case 1),  $1.2$  (Case 2),  $1.13$  (Case 3) and  $1.21$  (Case 4). For the pulsar parameters, we have used the values of the Vela pulsar;  $\tau = 70.6 \text{ s}^{-1}$ ,  $B_s = 6.68 \times 10^8 \text{ G}$ ,  $kT_s = 150 \text{ eV}$ , and  $A_s/A = 0.066$  (Ogelman, Finley & Zimmerman 1993), where  $B_s$  is the polar field strength, and  $A$  is the area of the stellar surface.

### 3.2 Vacuum gap

Before we investigate the electrodynamics of the non-vacuum gap, let us see some properties of the vacuum solution.

If the gap width  $W_{jj}$  along the magnetic field lines is much shorter than the trans-field thickness  $D_\perp$ , then the one-dimensional approximation works out well. From the one-dimensional Poisson equation,  $d\tilde{E}_{jj}/ds_{jj} = \tilde{B}_z$ , the inner and the outer boundaries satisfy

$$\int_{s_{jjin}}^{s_{jjout}} \tilde{B}_z ds_{jj} = 0; \quad (36)$$

where  $\tilde{B}_z$  is the dimensionless GJ charge density,  $s_{jjin}$  and  $s_{jjout}$  are the locations of the inner and the outer boundaries, respectively, in terms of the arc length along the field line from the stellar surface. In this case, the field-aligned electric field  $E_{jj}$  varies quadratically along the field lines such as one displayed in Fig. 7.

CHR pointed out that the trans-field thickness is suppressed by the pair creation, and postulated that the gap width is much longer the trans-field thickness,  $W_{jj} \gg D_\perp$ . By solving the Poisson equation with this slab-like geometry, they found that the inner boundary is located close to the null surface. While CHR solve the Poisson equation with a rectilinear geometry, the present model gives a vacuum solution with the dipole magnetic field in Fig. 2(a). The result retains a property of CHR; that is, the inner boundary is located near the null surface. This property does not depend on the location of the outer boundary.

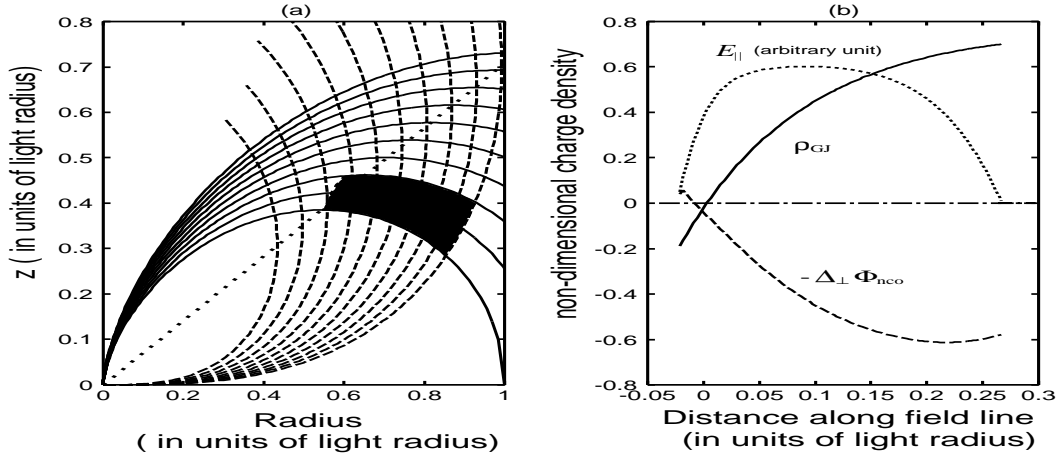


Figure 2. A solution of the vacuum gap. (a) The gap in the magnetosphere (lled region). The solid and dashed lines show the dipole eld lines and the curve lines that perpendicular to the eld lines, respectively. The dotted line is the null surface. (b) The solid, dashed, and dotted lines show the distributions of the G J density, the two-dimensional term, and acceleration eld, respectively, along a magnetic eld line.

In the elongated gap case, instead of the equation (36), the inner and the outer boundaries satisfy

$$\int_{s_{in}}^{s_{out}} (\nabla_{\perp}^2 \tilde{\Phi}_{nco} + \tilde{B}_z) ds_{jj} = 0; \quad (37)$$

where  $\nabla_{\perp}^2$  is the trans- eld part of the Laplacian. Fig. 2 (b) shows the distribution of  $\tilde{B}_z$ , the transverse term  $\nabla_{\perp}^2 \tilde{\Phi}_{nco}$ , and  $E_{jj}$  on a magnetic eld. The transverse term represents the effect of surface charge on the upper and the lower boundaries. From Fig. 2 (b), we find that the G J charge density and the transverse term almost balance out in most part of the gap,  $\tilde{B}_z \approx \nabla_{\perp}^2 \tilde{\Phi}_{nco}$ . Therefore, the distribution of  $E_{jj}$  has a plateau in the middle of the gap as the dotted line in Fig. 2 (b) shows.

### 3.3 Non-vacuum gap

In this subsection, we discuss the electrodynamics of the non-vacuum gap. The lowest order of the Fourier components of the two-dimensional term is represented by  $\nabla_{\perp}^2 \tilde{\Phi}_{nco} \approx \tilde{\nabla}_{\perp}^2 \tilde{\Phi}_{nco}$ , and therefore the two-dimensional term plays the role of a positive charge density in the gap.

#### 3.3.1 Electric eld structure

Fig. 3 shows the distributions of the eld-aligned electric eld  $E_{jj}$  along the magnetic eld lines. The solid, dotted and dashed lines represent, respectively, the electric eld on the magnetic eld lines threading the gap at 25, 50, and 75 % of the trans- eld thickness from

the lower boundary. The abscissa refers to the arc length from the null surface. The positive and the negative values indicate outside and inside, respectively, with respect to the null surface.

The variations of  $E_{\parallel}$  along the magnetic field line for all cases are similar to that for the vacuum case displayed in Fig. 2. In these cases, because the trans-field thickness is smaller than the gap width, the transverse term  $\nabla_{\perp}^2 \sim_{\infty}$  is important. The value of  $E_{\parallel}$  is determined in such a way that  $\nabla_{\perp}^2 \sim_{\infty}$ , the local charge density  $\sim$  and the GJ charge density  $B_z$  almost balance out in most part of the gap,  $\nabla_{\perp}^2 \sim_{\infty} \sim B_z$  (see Fig. 4). As a result, the distribution of the electric field shows a plateau in contrast with the quadratic shape (such as Fig. 7) in the one-dimensional model, in which the transverse term is ignored.

The effect of the external currents ( $j_1; j_2$ ) produces the difference in the distribution of  $E_{\parallel}$ . For example,  $E_{\parallel}$  on the plateau in Case 3 gradually decreases with the distance, while that in Case 4 gradually increases. In terms of  $j_1$  and  $j_2$ , the local charge density (27) is rewritten as  $\sim = B' (j_1 - j_2 + 2j) = j_{\parallel}$ , where  $j$  represents the current density carried by the positrons produced between the inner boundary and the position considered (e.g.  $j = 0$  at the inner boundary, and  $j = j_2$  at the outer boundary). For Case 3 ( $j_1 \neq 0; j_2 = 0$ ), the charge density at the outer boundary is  $B' (j_1 + j_2) = j_{\parallel}$ , indicating that the external positronic current  $j_1$  assists the current  $j_2$  in screening of  $E_{\parallel}$  at the outer boundary. Therefore, the strength of  $E_{\parallel}$  near the outer boundary is smaller than that near the inner boundary. In the same way, the external electric current  $j_2$  for Case 4 assists the screening of  $E_{\parallel}$  at the inner boundary, where the charge density is  $B' (-j_2 - j_2) = j_{\parallel}$ . Hence the strength of  $E_{\parallel}$  near the inner boundary is larger than that near the outer boundary. To be expected, if both the positronic and the electronic currents are injected the respective boundaries such as Case 2, these two contributions in the Poisson equation cancel each other, so that the plateau becomes almost flat.

Another effect of the external currents ( $j_1; j_2$ ) appears in the position of the inner boundary. The inner boundary for Case 3 is located outside of the null surface, and as a result the gap does not include the null surface, although the boundaries for the other cases are located inside of the null surface. This difference is discussed in §3.3.



### 3.3.2 Current density

The trans-eld structures found in the current density and the eld-aligned electric eld  $E_{\parallel}$  are summarized in Fig.5. The solid lines show the distribution of the current  $j_y$  across the eld lines. The maximum value (arbitrary units) of  $E_{\parallel}$  on each eld line is also plotted in Fig.5.

We find that maximum value of  $j_y$  for each case is  $j_{y, \text{max}} = 0.2$  (Case 1),  $0.17$  (Case 2),  $0.07$  (Case 3) and  $0.3$  (Case 4). The total current density on each magnetic eld line is represented by  $j_{\text{tot}} = j_y + j_1 + j_2$ . In Case 1, for example, because no particles come into the gap through both the boundaries, (i.e.,  $j_1 = j_2 = 0$ ), the total current is carried only by the pairs produced in the gap, that is,  $j_{\text{tot}} = j_y$ . The total current densities at the maximum are  $j_{\text{tot}} = j_{y, \text{max}} = 0.2$  (Case 1),  $j_{y, \text{max}} + j_1 + j_2 = 0.37$  (Case 2),  $j_{y, \text{max}} + j_1 = 0.17$  (Case 3), and  $j_{y, \text{max}} + j_2 = 0.4$  (Case 4).

As mentioned in §3.1, the solution disappears if  $j_y$  exceeds the critical value because the super-GJ region becomes dominant in the gap so that the eld-aligned electric eld changes its direction. However, it is noteworthy that the values  $j_y$  for Case 1, Case 2 and especially Case 4 exceed the critical value ( $\approx 0.1$ ) of the previous one-dimensional model. As an effect of the trans-eld structure, the transverse term  $\nabla_{\perp}^2 \sim n_{\text{co}}$  behaves as the positive charge. Therefore, if the super-GJ points appear in the negatively charged region, the effect of it in the Poisson equation can be reduced by the transverse term. In Case 4, for example, the super-GJ points tend to appear in the negatively charged region around the inner boundary due to the external electric current  $j_2$  (see Fig.4). Then, we find that the shape of its inner boundary (see next subsection) and the gap structure are formed so that the transverse term cancels the super-GJ points as Fig.4 shows. Because we increase  $j_y$  until the transverse term marginally sustains the super-GJ region, we obtain the critical value ( $\approx 0.3$ ) of Case 4 increasing significantly from the one-dimensional one ( $\approx 0.1$ ). The situation such as Case 4 is very important for obtaining the solution of the increased current. On the contrary, if the super-GJ space charge density appears near the outer boundary, it is positive, so that the transverse term does not reduce the super-GJ charge density but the opposite. In such a case (e.g. Case 3 with positive external current), the critical current density is rather small.

In the outer gap model by CHR, the pairs are supposed to be created much in the convex side (i.e. in the upper half), and a large current flows there, while they assumed the vacuum region in the lower half. This type of gap is realized in Case 1 by assuming no

external currents. From the panel for Case 1 in Fig. 5, we find that the vacuum-like region occupies a lower half of the gap, and the current-carrying (non-vacuum) region is restricted in the upper half region. As far as the trans-field structure is concerned, our electrodynamic model reproduces the structure similar to that assumed in CHR. However, the location of the inner boundary manifests itself in different manner, as shall be shown in the next subsection.

Fig. 5 shows that the current  $j_y$  increases with increasing height, and then decreases. The increase is simply because the  $\gamma$ -rays propagate the convex side of the field lines and make pairs. The decrease is caused by the following effects. Firstly, the upper part is illuminated mainly by the  $\gamma$ -rays which were radiated in the middle region, while almost of the  $\gamma$ -rays emitted at the lower half part escape through the inner or the outer boundaries before reaching the upper region. Secondly, the field-aligned electric fields, the Lorentz factor ( $\gamma/E_{jj}^{1=4}$ ) and in turn the energy of the emitted  $\gamma$ -rays ( $\propto E_{jj}^{3=4}$ ) decrease with increasing of the height in the upper half region. Furthermore, the threshold energy of the X-rays colliding with the low-energy  $\gamma$ -rays moves to the Wien region of the Planck law, and thereby, the mean free path of the  $\gamma$ -rays sharply increase with decreasing of its energy. By combinations of these effects, the current density  $j_y$  decreased with increasing of the height in the upper half region.

In contrast, the exponential increase of the currents near the upper boundary are predicted in CHR. This case may be obtained, if one takes non-thermal X-ray fields with a modest power-law index such as the Crab pulsar, or if one considers a case in which the strength of  $E_{jj}$  is ineffective to the Lorentz factor and the energy of the  $\gamma$ -rays (e.g. the unsaturated motion of particles). These possibilities are investigated in the subsequent papers.

### 3.3.3 Location of the inner boundary

The filled regions in Fig. 6 show the shape of the gap. The beak-like shape of the inner boundary is remarkable when one compares it with that of the vacuum case. The magnetic field line on which the current density  $j_y$  is maximized at  $j_{max}$  runs through the cusp of the beak.

An important feature of the external currents ( $j_1; j_2$ ) appears in the position of the inner boundary of the lower end part, where few pairs are produced. If  $j_1$  and  $j_2$  are equal such as Case 1 and Case 2, the inner boundary is located close to the null surface. If  $j_1$  and  $j_2$  are

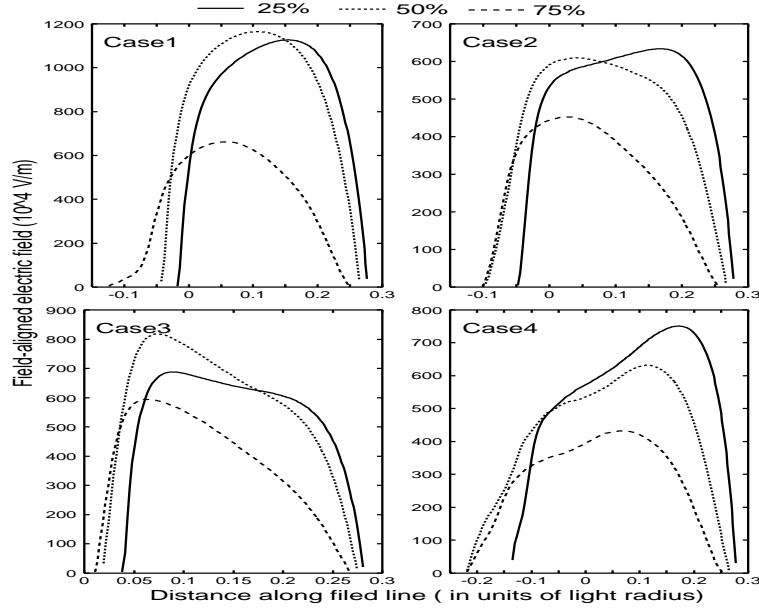


Figure 3. The electric field structure for Case 1, Case 2, Case 3, and Case 4. The solid, dotted, and dashed lines show the distributions of the field-aligned electric field on the three different magnetic field lines, which locate, respectively, 25, 50, and 75% of the gap trans- field thickness measured from the last open field line. The abscissa represent the arc length with the origin at the null surface.

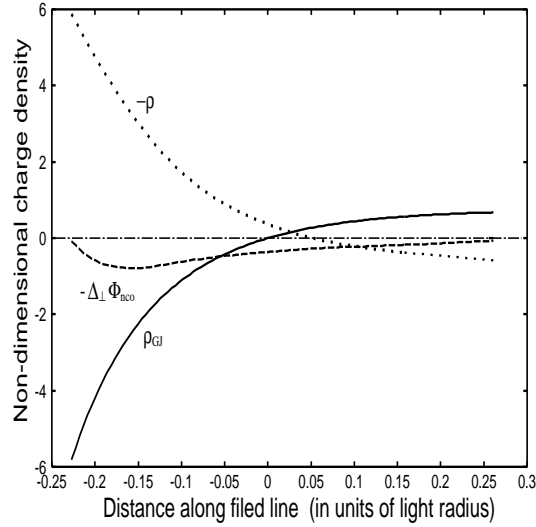


Figure 4. The distributions of the GJ charge density (solid line), the transverse term (dashed line) and the space charge density (dotted line) on the magnetic field line, on which  $j_{\parallel} = j_{\parallel \max}$  for Case 4.

not equal such as Case 3 and Case 4, on the other hand, the inner boundary shifts outside or inside. This is because the effective charge neutral shifts relative to the conventional null surface by the space charge caused by the external current. This effect is originally pointed out by the one-dimensional model of Hirota & Shibata (2001).

As mentioned above, the inner boundary at the lower part region of Case 1 comes to close the null surface. On the other hand, we find that the inner boundary at the cusp,

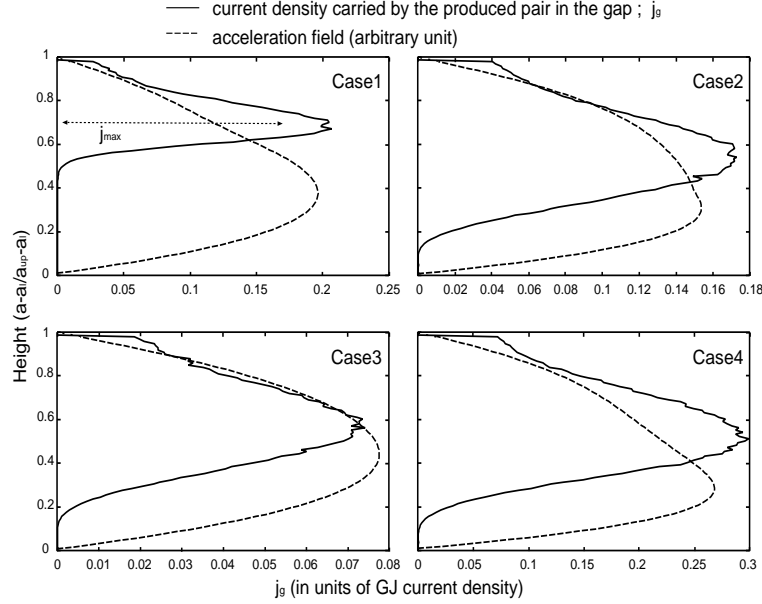


Figure 5. The transverse distribution of the current density and the acceleration field. The solid line shows the transverse distribution of the current  $j_{\parallel}$  carried by the pairs produced in the gap. The dashed line shows the maximum value (arbitrary units) of  $E_{\parallel}$  on each field line.

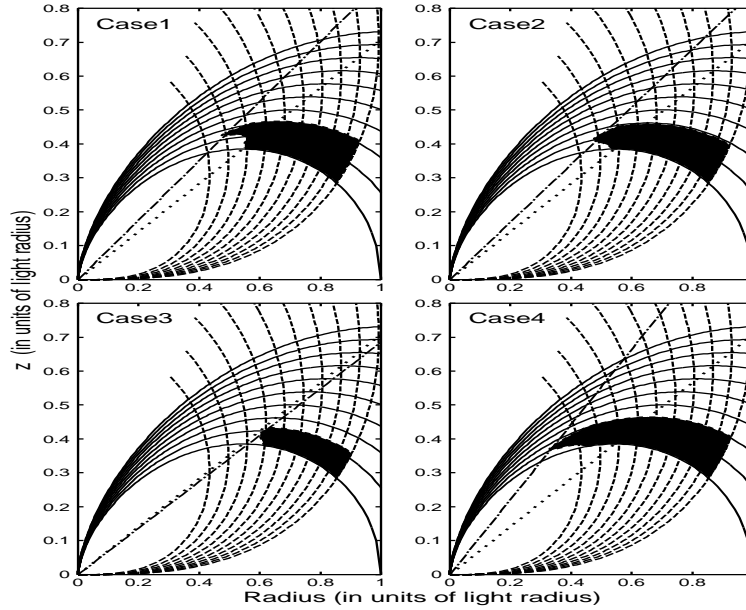


Figure 6. The geometry of the outer gap (shaded region in each panel). The solid and dashed, and dotted lines are the same as Figure 2. On the dashed-dotted line in each panel, the condition,  $j_{\parallel, \text{max}} + j_{\perp} = E_z = E^*$ , is satisfied (see text).

where  $j_{\parallel} = j_{\parallel, \text{max}}$ , leaves from the null surface and moves toward the stellar surface. Let us investigate this displacement. From the stability condition discussed in xx2.4, we have

$$\frac{\partial E_{\parallel}}{\partial s_{\parallel}} = 4\pi \tilde{n}_{\infty} + E^* (j_{\parallel} - j) = j_{\parallel} + E_z > 0: \quad (38)$$

With the help of  $E_z = E^*$  and the fact that both  $4\pi \tilde{n}_{\infty} = 0$  at the end  $j_{\parallel} = 1$  hold on the cusp, we have

$$(j_{nax} + j_2 - j) \leq B_z(r_{in}) = B(r_{in}) \leq 1; \quad (39)$$

where we have used the fact that  $j_+ - j$  becomes  $j_1 - j - j_{nax}$  at the cusp. This condition indicates that the inner boundary is located between the stellar surface where  $B_z = B = 1$  and the position on which the local charge density caused by the longitudinal currents equals the G J charge density.

In Case 1 and Case 2, because  $j_1$  equals  $j_2$ , the condition (38) becomes

$$j_{nax} \leq B_z(r_{in}) = B(r_{in}) \leq 1: \quad (40)$$

The dashed-dotted lines for Case 1 and Case 2 in Fig.6 show the positions on which the condition  $j_{nax} = B_z = B$  ( $j_{nax} = 0.2$  in Case 1 and  $j_{nax} = 0.17$  in Case 2) is satisfied. We find that the cusp is located significantly closer to the position where the space charge density,

$j_{nax} B$ , equals the G J charge density,  $B_z$ . Noting that  $B_z = B$  increases with decreasing of  $r$ , we expect that the cusp shifts toward stellar surface as  $j_{nax}$  increases. If the current carried by the particles produced in the gap were the G J value (i.e. if  $j_y = 1$ ), the cusp would be located on the stellar surface, and therefore the outer gap would start from the stellar surface. However, because we have no solution if  $j_y$  exceeds a critical value ( $\approx 0.2$  for Case 1), we do not obtain the solution in which the inner boundary touches the stellar surface.

For Case 3 and Case 4, the condition (39) is rewritten as  $(j_{nax} - j) \leq B_z(r_{in}) = B(r_{in}) \leq 1$  and  $(j_{nax} + j_2) \leq B_z(r_{in}) = B(r_{in}) \leq 1$ , respectively. The dashed-dotted lines in the lower panels of Fig.6 show the positions which satisfy the condition  $(j_{nax} - j)B = B_z$  for Case 3 and  $(j_{nax} + j_2)B = B_z$  for Case 4. Such as Case 1 and Case 2, the cusps in these cases also take the position on which the space charge density equals the G J charge density. Thus, we find that the outer gap extends from the point on which the charge density caused by the longitudinal current made up of  $(j_{nax}; j_1; j_2)$  equals the G J charge density.

#### 4 DISCUSSION

We have studied the electrodynamics of the outer gap including the trans-eld structure in the meridional surface. We have found that the inner boundary shifts toward the stellar surface from the null surface as  $j_y$  or  $j_2$  increases, and forms the beak shape, which was found in the vacuum gap geometry. We have shown the specific solution, of which the

current density  $j_y$  carried by the particles produced in the gap becomes significantly larger than the upper limit given by the one-dimensional model ( $j_y \leq 0.1$ ).

#### 4.1 Comparison with previous works

After CHR, the traditional shape of the outer gap have been based on the vacuum model, in which the gap extends between the null surface and the light cylinder. Although the traditional outer gap models have been successful in explaining overall features of the observed light curves (e.g. double-peaks in one period, and the presence of the bridge emission), the model cannot account for the presence of the outer-wing emission and of the  $\gamma$ -pulse emission from the Crab pulsar. Recently, the caustic model by Dyks & Rudak (2003), and Dyks, Harding & Rudak (2004) reproduces the observed light curves better than the traditional outer gap model. The caustic model demanded that the emission region extends from the polar caps to the light cylinder. But, the reason that the gap extends on both sides of the null surface is not evident. Our two-dimensional electrodynamic model indicates that if a marginal stable condition,  $(j_y + j_z - j)\tilde{B}(\text{in}) = \tilde{B}_z(\text{in})$  holds, then the inner boundary shifts toward the stellar surface as  $j_y$  and  $j_z$  increase.

We have actually demonstrated that the gap extends on both sides of null surface in Case 4 (Fig. 6), in which the electrons come into the gap through the outer boundary. In the global magnetospheric models (e.g. Mestel et al. 1985, Shibata 1995), the electrons circulate the magnetosphere globally and turn back into the outer gap. Although the observed light curves may be reproduced better by assuming the injection of the electrons at the outer boundary ( $j_1 = 0; j_2 \neq 0$ ), it is not certain whether the injection from the outer boundary is favored for reproducing the  $\gamma$ -ray spectrum. This will be studied in a subsequent paper. It is notable that, in the one-dimensional model, the observed spectra have been reproduced by assuming the injected positrons from the inner boundary (Hirotani et al. 2003; Takata et al. 2004).

Although the present model is very simple, we must argue that two or three dimensional model will open a way to diagnose the current system in the outer gap when the observed phase resolved  $\gamma$ -ray spectra and light curves are compared with the model predictions. The external currents ( $j_1; j_2$ ) strongly control the  $\gamma$ -ray spectrum by changing the electric field strength. On the other hand, the current density  $j_y$  and its distribution across the field lines reflect the pulse shapes through the location of the gap boundary. Thus, combining the

spectra and the pulse shapes, the electrodynamic model enables us to know the current system in the outer gap.

#### 4.2 Outside of the gap

In this subsection, we discuss the dynamics in outside of the gap. We shall show that co-existence of low energy particles and the high energy particles streaming from the gap is required to hold the idealMHD condition,  $E_{\parallel} = 0$ , in the outside of the gap. We shall lead this conclusion with the reductio ad absurdum.

Taking Case 1 ( $j_1 = j_2 = 0$ ), let us consider the region between the stellar surface and the inner boundary. We assume at the moment that only the electrons escaping from the gap exist in that region and migrate toward the stellar surface. The Poisson equation and the energy conservation for the electrons in the one-dimensional form are

$$\frac{d\tilde{E}_{\parallel}}{ds_{\parallel}} = \frac{0}{D_{\infty}^2} - \frac{j_2 \tilde{B}}{s_{\parallel}} + \tilde{B}_z; \quad (41)$$

and

$$\frac{d}{ds_{\parallel}} = \tilde{E}_{\parallel}; \quad (42)$$

respectively, where  $s_{\parallel}$  is the arc length along the eld line from the stellar surface,  $0$  is the Lorentz factor of the particles on the inner boundary, and  $\gamma = 1 = \sqrt{1 - \frac{v_{\infty}^2}{c^2}}$ . The first term in the right hand side of the equation (41) represents the two-dimensional effect.

Near the inner boundary but outside of the gap, because  $s_{\parallel} \ll 1$  and because  $0$ , the equation (41) can be rewritten as  $d\tilde{E}_{\parallel}/ds_{\parallel} = -j_2 \tilde{B} + B_z$ . Since  $j_2 \tilde{B} \ll B_z$  is satisfied, we find  $d\tilde{E}_{\parallel}/ds_{\parallel} > 0$ , where the equality is satisfied on the inner boundary. By noting  $E_{\parallel} = 0$  on the boundary by the definition, the eld-aligned electric eld has the negative sign in the outside of the gap, so that the Lorentz factor of the escaping electrons decreases. If the decrease of  $\gamma$  from  $0$  becomes a considerable value, the transverse term dominates the right hand side of equation (41). This transverse term causes further decrease of  $\gamma$  and subsequent exponential development of the Lorentz factor. Thus, we find that the idealMHD condition does not hold between the inner boundary and the stellar surface. On these ground, we conclude that other electrons populate between the stellar surface and the inner boundary to hold the condition  $E_{\parallel} = 0$  (i.e. the idealMHD condition). These electrons will be supplied from the stellar surface or the electronic cloud on the polar caps by the negative eld-aligned electric eld, which will appear unless there are such electrons.

The same argument is applied for outside of the outer boundary, and therefore the ions (or positrons) in addition to the positrons escaping from the gap are required.

#### 4.3 Displacement of the outer boundary

In all the four cases in §3, we assume that each position of the outer boundary is located far outside from the null surface. Then expansion of the gap in the trans-field direction is suppressed by the pair creation. As a result, the trans-field thickness  $D_\perp$  becomes shorter than the gap width  $W_{\text{gj}}$ .

In our model, the location of the outer boundary  $r_{\text{out}}$  is free (§2.4), but determine the value of the total current running through the gap. We may put the outer boundary near the null surface. In such cases, because  $W_{\text{gj}}$  is short, we have a gap which has a larger  $D_\perp$  than those of Case 1–Case 4. In this wedge-like gap, because the trans-field propagating distance of the  $\gamma$ -rays in the gap is negligible as compared with  $D_\perp$ , the magnetic field lines are effectively straight in the gap. We then anticipate that the solution of our two-dimensional model with this geometry is effectively the same as that of the one-dimensional model.

Fig. 7 shows a solution of the wedge-like gap, where the model parameters  $j_1 = j_2 = 0.1$ , which are the same as Case 2. As a result, there is no solution if  $j_2$  becomes greater than 0.1, which is smaller than the critical value of 0.17 for Case 2. Furthermore, the distribution of the field-aligned electric field is quadratically, and is different from one of the slab-like gap such as Case 1–Case 4.

#### 4.4 Drift motion

Let us examine validity of the assumption that the non-corotational drift motion is negligible as compared with the corotational motion. From equation (12), the drift motion around the rotational axis may be expressed as

$$\mathbf{v} = \mathbf{\Omega} \times \mathbf{r} + c \frac{\mathbf{E}_\perp}{B}; \quad (43)$$

where  $\mathbf{E}_\perp = -\nabla \phi_{\text{nc}} = -\nabla \phi_2$ . The first and the second terms of the right hand side of the equation (43) represent the corotational and the non-corotational motion, respectively. Fig. 8 shows the drift velocity of the non-corotational part evaluated on the outer boundary. The plus (or minus) sign for the abscissa represents the direction (or counter-direction) of the stellar rotation. From this figure, we find that the drift motion becomes super-corotation in the lower part of the gap, and sub-corotation in the upper part. In our calculation, we find



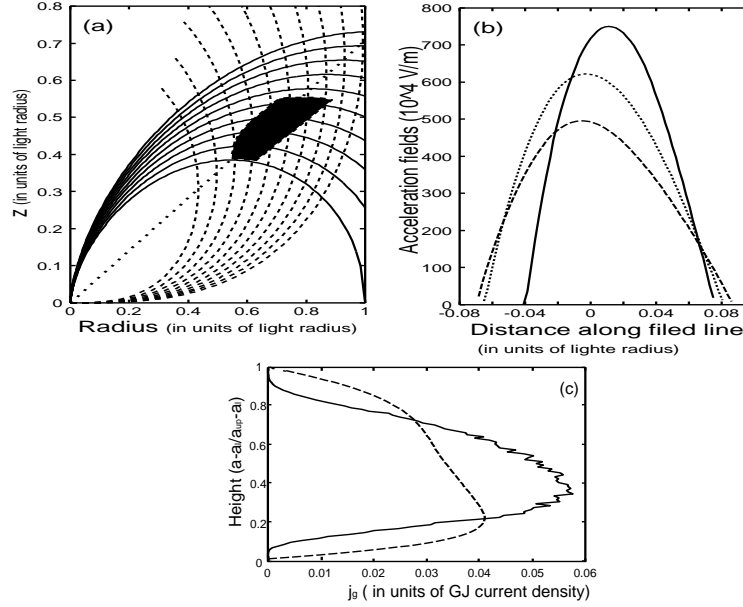


Figure 7. A solution of the wedge-like gap. The external currents  $(j_1; j_2) = (0.1; 0.2)$  is the same as Case 2. (a) The geometry of the outer gap (dark region). The solid, dashed, and dotted lines are the same as in Fig. 6. (b) The distribution of the field-aligned electric field. The solid, dotted, and dashed lines are the same as in Fig. 3. (c) The trans-eld structures of the current and the field-aligned electric field. The solid and dashed lines are the same as in Fig. 5.

that non-corotational motion is a few per cent of the corotational motion (i.e.  $\beta_{\infty} \approx \beta_2$ ). The rotational period  $\hat{P}_3$  of drift motion of plasma due to  $E_{\parallel}$  in the outer gap is suggested to be  $\hat{P}_3 \approx 13P_1$ , where  $P_1$  is the corotational period, and we used the maximum drift velocity  $|v| \approx 0.06c$  at  $\theta = 0.8\theta_{lc}$ . Since we have neglected the structure of the azimuthal direction, we cannot calculate the drift velocity due to the azimuthal electric field. However, we may anticipate that the strength of the azimuthal electric field are same order (or less) as compared with the values of the trans-eld electric field  $E_{\perp}$ , unless the dimension in the azimuthal direction is much smaller than that in the meridional plane. Therefore, we safely neglect the non-corotational drift motion.

In the polar cap model of Ruderman & Sutherland (1975), the subpulse drift of the radio band is attributed to  $\partial E_{\perp} = B$  drift in the polar cap region. The sub-pulse drifts have been observed from the old pulsars such as PSR B0943+10 ( $\hat{P}_3 = P_1 \approx 37.35$ ), B0826-34 (14), B2303+30 ( $\approx 23$ ), B0031-07 ( $\approx 34$ ) (Gil, Melikidze & Geppert 2003). The pulsars quoted are old ( $\approx 10^7$ yr) and slow ( $P \approx 1$ s) pulsars with spin-down energy many orders of magnitude less than known  $\gamma$ -ray pulsars ( $\approx 10^6 - 10^8$ yr). Even though the pulsar is old, the magnetic pair creation process in polar cap region must take place due to the high magnetic field ( $B_s \approx 10^{12}$ G). In the outer gap of such old pulsars, it is not clear whether the

high energy radiation and the photon-photon pair creation process take place efficiently. In following, therefore, we investigate the outer gap of the old pulsars.

For simplicity, we assume that the available potential drop,  $\Phi_a = B_s^2 R^3 / 2c^2$ , on the stellar surface is used only for the acceleration of particles in the outer gap. This assumption is not valid for the young fast pulsars, but not bad for the old and slow pulsars because the gap covers the almost pulsar magnetosphere. The corresponding Lorentz factor will be estimated from  $m_e c^2 \gamma_a = e \Phi_a$ , to be  $\gamma_a \approx 2.5 \times 10^6 P^{-1.5} \dot{P}_{15}^{-0.5}$ , where  $P$  is the stellar rotation period in units of 1s, and  $\dot{P}_{15}$  is the period derivative in units of  $10^{-15} \text{ s}^{-2}$ . The pair creation condition is  $E \geq E_X + 2(m_e c^2)^2$ , where  $E_X$  is the energy of the soft photons, and  $E$  is the curvature photon energy, which is  $E = 0.1 P^{-5.5} \dot{P}_{15}^{-1.5} \text{ GeV}$ , where we adopt the light radius as the curvature radius of the magnetic field lines. From this condition, the threshold energy of soft photons in terms of  $P$  and  $\dot{P}_{15}$  becomes  $E_X \approx 5 P^{5.5} \dot{P}_{15}^{-1.5} \text{ keV}$ . For any neutron star cooling models and the polar-cap heating models, such high thermal temperature for old slow ( $P \approx 1 \text{ s}, \dot{P}_{15} \approx 1$ ) pulsars is not predicted (Zhang et al. 2004, and references therein). For checking, we applied the present numerical code for an older pulsar PSR 0943+10 with the X-rays field of an unexpectedly temperature, which we adopted for Vela pulsar ( $E_X \approx 0.15 \text{ keV}$ ). We found that no pairs are produced in the gap. On these ground, we conclude that the pair creation process does not take place in the outer gap of the old pulsars quoted above.

Such silent gap does not produce current carrying particles by itself. However if the external current comes into the gap through the boundaries, the electrons (or positrons) are accelerated in the gap, and then radiate curvature photons (for example, the energy of the  $\gamma$ -rays is about  $E \approx 100 \text{ MeV}$  with  $P \approx 1 \text{ s}$  and  $\dot{P}_{15} \approx 1$ ). If the external current has the Goldreich-Julian value  $B_s^2 R^3 = c$ , then the luminosity is same order of the spin down energy, namely  $L \approx \dot{E}_J \approx \frac{B_0^2}{4} R^6 \dot{\Omega}^3$ . For example, the predicted luminosity for PSR B0826-34, the observed distance ( $d \approx 0.54 \text{ kpc}$ , Lyne & Smith 1998) of which is the nearest in the pulsars quoted above, is  $6.2 \times 10^{30} \text{ erg/s}$ . However, since the corresponding flux on Earth,  $F = L / 4d^2$ , is  $2 \times 10^3 \text{ erg/cm}^2 \text{ s}$ , which is below sensitivity of and unobservable even with the new  $\gamma$ -ray telescope GLAST. On the other hand, the middle age pulsars ( $\approx 10 \text{ yr}$ ) will have the gap in which both of the pair creation and the  $\gamma$ -ray radiation processes take place, and are interesting candidates for GLAST (Torres & Nuza 2003).

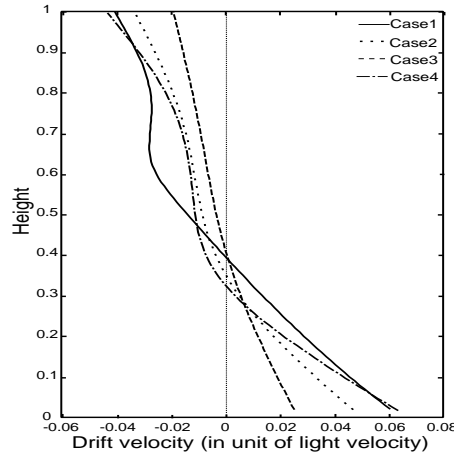


Figure 8. The non-rotational drift motion around the rotation axis on the outer boundaries. The solid, dotted, dashed, dashed-dotted correspond to the Case 1, 2, 3, and 4, respectively. The abscissa is the drift velocity in units of light velocity.

## ACKNOWLEDGMENTS

We are grateful to Dr Motokazu Takizawa for fruitful discussions. Authors also thank Dr Geoffrey Wright, the referee, for insightful comments on the manuscript.

## REFERENCES

- Cheng K. S., Ho C., Ruderman M., 1986, *ApJ*, 300, 500
- Cheng K. S., Ruderman M., Zhang L., 2000, *ApJ*, 537, 964
- Dyks J., Rudak B., 2003, *ApJ*, 598, 1201
- Dyks J., Harding A. K., Rudak B., 2004, *ApJ*, 606, 1125
- Gil J., Melikdze G. I., Geppert U., 2003, *A & A*, 407, 315
- Goldreich P., Julian W. H., 1969, *ApJ*, 157, 869
- Hirota K., 2003, *Progress in Astrophysics Researches*, vol.1 (Nova Science)
- Hirota K., Shibata S., 1999, *MNRAS*, 308, 54
- Hirota K., Shibata S., 2001, *MNRAS*, 325, 1228
- Hirota K., Harding A. K., Shibata S., 2003, *ApJ*, 591, 334
- Lyne G. A., Smith F. J., 1998, *Pulsar Astronomy*, Cambridge astrophysics series, Cambridge Univ. Press, Cambridge
- Mestel L., 2003, *Stellar Magnetism*, International Series of Monographs of Physics. Oxford Univ. Press, Oxford
- Mestel L., Robertson J. A., Wang Y., Westfold K. C., 1985, *MNRAS*, 217, 443
- Michel F. C., 1979, *ApJ*, 227, 579

- Michel F. C., Li H., 1999, *Physics Reports*, 318, 227
- Ogelman H., Finley J. P., Zimmerman H. J., 1993, *Nat*, 361, 136
- Roman R. W., 1996, *ApJ*, 470, 469
- Roman R. W., Yedigözü I. A., 1995, *ApJ*, 438, 314
- Ruderman M. A., Sutherland P. G., 1975, *ApJ*, 196, 51
- Shibata S., 1995, *MNRAS*, 276, 537
- Sturrock P. A., 1971, *ApJ*, 164, 529
- Takata J., Shibata S., Hirokani K., 2004, *MNRAS*, 348, 241
- Thompson D. J., et al., 1999, *ApJ*, 516, 297
- Torres D. F., Nuza S. E., *ApJ*, 583, L25
- Zhang L., Cheng K. S., Jiang Z. J., Leung P., 2004 *ApJ*, 604, 317